Terrain-Moisture Classification Using GPS Surface-Reflected Signals

Michael S. Grant, Scott T. Acton, *Senior Member, IEEE*, and Stephen J. Katzberg

***Abstract*— In this study we present a novel method of land surface classification using surface-reflected GPS signals in combination with digital imagery. Two GPS-derived classification features are merged with visible image data to create *terrain-moisture* (TM) classes, defined here as visibly identifiable terrain or landcover classes containing a surface/soil moisture component. As compared to using surface imagery alone, classification accuracy is significantly improved for a number of visible classes when adding the GPS-based signal features. Since the strength of the reflected GPS signal is proportional to the amount of moisture in the surface, use of these GPS features provides information about the surface that is not obtainable using visible wavelengths alone. Application areas include hydrology, precision agriculture, and wetlands mapping.**

I. Introduction

USE of the Global Positioning System (GPS) satellite L-band (1.57542 GHz) coarse acquisition (C/A) signal for ocean windspeed measurement and land-surface remote sensing has been under development since the mid-1990's. [1][2][3]. In this study we present a novel use of the GPS surface-reflected signal for terrain/land cover classification based on both the visible attributes and the moisture content of the surface.

GPS remote sensing generally involves use of the direct satellite signal to obtain both instrument (receiver) position and signal strength information while simultaneously measuring the strength of the surface-reflected signal (Fig. 1). To compute the surface coordinates of the area being sensed, the signal *specular* (mirror-reflection) point, *S*, is determined from the known aircraft position, satellite position and elevation angle (γ), along with surface topographical data (digital elevation models). Surface remote sensing occurs along the *specular point ground track*, P_s, created as the aircraft flies at altitude, *h*, above the surface. Given generally specular reflection (vs. diffuse scattering) of the GPS signal from the terrain, the ground track is approximately one *Fresnel zone* [4] in width (point *P*).

During data acquisition, the NASA-Langley GPS remote sensing (GPSRS) instrument used in this study simultaneously correlates (compares) the unique satellite pseudo-random noise (PRN) code in a given satellite signal with an instrument-generated copy of the code. For each surface measurement, the reflected signal is correlated at 14 successive delay times (or *delay bins*) relative to the arrival of the signal from the specular point. The correlation results are squared as part of instrument signal processing and recorded for later analysis. During post-processing, an ideal, squared-correlation function (λ^2 waveform) is fitted to each set of delay bin values, as shown in Fig. 2. The estimated peak, K_R, is proportional to surface-reflected power. Similar processing of the direct signal produces instrument output, K_D, proportional to direct signal power.

Surface reflectivity, *R*, is the ratio of reflected power to direct power [5], and is computed using GPSRS measurements by:

$$R = \frac{K_R - \bar{n}}{K_D} f_c \,, \tag{1}$$

where $\bar{n}$ is average instrument noise and f_c is a calibration scale factor. Constant f_c is calculated using over-water values of K_R and K_D and the known reflectivity of water (R ~ 0.61) [5]. It has been well established that microwave energy in the wavelength range of the GPS C/A signal is reflected from a land surface (e.g. a field) to a greater extent as the moisture content increases [6][7]. We therefore utilize reflectivity, *R*, as one of two GPS-based classification features.

Additionally, it is known that certain types of terrain (including the vegetation) scatter radio frequency (RF) signals more than others [4][5]. In the GPSRS, this increased scattering results in a "widening" of the [sampled] correlation waveform as compared to the ideal λ^2 waveform. In this study we introduce a measure of this widening effect called the signal *dispersion*, *D*, defined as:

$$D \equiv \sum_{i=0}^{B-1} w_i L_{j+i} \,, \tag{2}$$

with linearly increasing weights, w_i:

$$w_i = \{0,1,\ldots,B-1\} \,, \tag{2a}$$

where L_j is the normalized, squared-correlation sample at the j^{th} delay bin, j = {1,2,…,14}. A given measurement will have *B* correlator outputs (B ≤ 14) that are above the noise threshold. On average, a rougher surface will have a larger dispersion value than a relatively smooth one. This allows use of dispersion, *D*, as a second GPS-based surface classification feature.

The reflectivity and dispersion measures are used to discriminate terrain (or ground cover) types which have generally different surface/soil moisture (SM) levels. Using GPS-derived classification features along with aerial imagery, various terrain classes can be differentiated based on both visible characteristics and moisture content. This leads to the notion of a *terrain-moisture* (TM) class; one with a visible terrain/landcover type combined with a moisture component. An example TM class is: 'pasture - 11% soil moisture'. More generally, the moisture component may be given in terms of the amount of precipitation received, e.g. 'desert scrubland – 5 mm precipitation.'

We note that *unsupervised* terrain classification (i.e. data clustering followed by labeling) using GPS surface reflectivity in combination with black and white imagery was introduced in our earlier work [8]. Here we perform *supervised*, (maximum-likelihood) classification with data vectors

comprised of three visible bands (red, green, blue) and two GPS classification features. To our knowledge, this is the first effort to develop GPS signal-derived classification features that, together with visible imagery, allow land surface types to be distinguished using both visible characteristics and relative moisture content.

II. Study Region and Methods

We acquired GPS data and surface imagery in an area near Tifton, Georgia during the joint NASA-Department of Agriculture Soil Moisture Experiments 2003 (SMEX03) study. The GPSRS instrument was flown aboard a Cessna aircraft equipped with a down-looking, digital camera to obtain contemporaneous imagery. With the research aircraft in this configuration, both high-resolution imagery and GPS data over the region of interest could be obtained in relatively close time proximity (or simultaneously if desired), to avoid the longer time differences (several days or weeks) that often result when utilizing available, cloud-free satellite imagery with data from aircraft-based sensors. At intervals during the June/July study period, surface moisture measurements at a number of field sites were obtained by hydrology researchers.

We focus on four sites, designated GA23, GA27, GA34, and GA36, within the Tifton study area. Aerial imagery of these sites was acquired on 6/28/03. GPS remote sensing data from these sites were acquired a few hours after a rain event on 6/30/03. Sites GA23 and GA34, in the northern part of the study area received between 6 mm and 13 mm of precipitation, respectively, on the morning of 6/30/03. The more southerly sites, GA27 and GA36, received no rain during the week prior to data acquisition. Fig. 3 gives average surface reflectivity (eqn. 1) for each site along with measured soil moisture at the 0 – 3 cm and 3 – 5 cm depths.

The high-resolution (~ 0.25 m) images obtained for each site were geolocated (registered) to 1 m resolution black & white orthoquad imagery of the area and then re-sampled to 1 m resolution to aid in processing. As part of the signal calibration process, small misalignments in the GPSRS data specular point position on the surface due to DEM and aircraft position uncertainty were corrected by aligning the data to visible surface features. Manual segmentation and data labeling of site images using visibly identifiable classes was performed to obtain classifier training data and to allow classification accuracy to be assessed. For ground truth data labeling, the visible classes identified (e.g. 'bare field,' 'pasture,' 'forest,' etc.) at a particular site were assumed to be at a uniform soil moisture (SM) level. Sites images and associated truth segmentation maps of GA23 (Fig. 4 top row) and GA34 (bottom row) are representative. Each site has between 5 and 10 visible classes which, with 4 distinct SM levels, results in 32 separate TM classes among all four sites. Examples include: 'Pasture – 2.2 to 4.7%' (P2), 'Bare Field – 8.7 to 10.1%' (BF8), and 'Mixed Forest/Pasture – 11.5 to 12.2%' (MFP11).

The measured reflectivity and dispersion values covering all the sites were scaled to the digital image data range of 0 – 255 prior to classification. Various scene classifications were performed using either the [digital image] visible bands (V) alone, or visible bands plus reflectivity (VR), or visible bands plus reflectivity and dispersion (VRD). Sites were classified both individually, to categorize visible classes at the *same* SM level, and in pairs, to determine how well common visible classes at two *different* SM levels could be distinguished. Occasional cloud cover resulted in varied illumination of the same visible classes (e.g. 'bare field', 'forest') at different sites. To reduce the effect of differing light levels when classifying a pair of sites, image data samples from the landcover classes common to both sites were used for classifier training data. The accuracy of classification for a given class is defined here as the percent of correctly classified pixels as compared to the segmentation map. Overall classification accuracy is the average over a set of classes.

III. Results

Results are given here in summary form. With the exception of the 'Mixed Forest/Pasture,' (MFP) class, for the individual sites (at a uniform SM level) classification was improved by the addition of GPS features; particularly for classes which could not be discriminated well using only image data. The MFP classification accuracy was relatively low when using only image data (~ 16%) and/or tended to degrade slightly with the addition of the GPS features. From Table I, with MFP removed the average classification accuracy of GA23 (i.e. for all classes in the site) was the most improved when combining GPS with image data as compared to using imagery alone, whereas GA34 showed the least overall improvement. The effectiveness of the added GPS features tended to increase when classifying more complex scenes with larger numbers of visible classes. GA34 contains 5 visible classes, GA36 and GA27 each have 7, and GA23 has 10 such classes.

Comparing sites with common visible classes but with *different* SM levels illustrates the concept of partitioning a scene into *terrain-moisture* classes. By definition, physically distinct regions in the same visible class (e.g. 'Emergent Field') cannot be distinguished based on [invisible] sub-surface moisture level using image data alone, regardless of any incidental differences such as illumination level or vegetation coverage. We thus compare the performance of adding one (VR) or both (VRD) GPS features to the visible wavelength data. A typical result is shown in Fig. 5 where GA23 and GA34 are classified jointly, for the visible class regions which are common to both sites. Clearly, some classes were more accurately classified than others. Addition of the dispersion feature (VRD) increased the classification accuracy by an average 9.4% over the visible plus reflectivity case (VR). Without the difficult to resolve 'MFP' class, on average the dispersion feature improved the classification accuracy by 10.7%.

IV. Conclusions

We have demonstrated that the terrain/land-cover classification accuracy of visibly identifiable classes at a single moisture level can be improved by utilizing GPS-derived classification features in combination with visible wavelength imagery. Significantly increased classification accuracy of individual sites due to added GPS features was

not, apparently, a function of soil moisture level or of the amount of precipitation preceding data acquisition. Additionally, it was demonstrated that for sites with generally *different* moisture levels but having common *visible* classes, remotely sensed areas can be partitioned into *terrain-moisture* (TM) classes. This capability was observed even for sites such as GA23 and GA27, which had relatively little difference in soil moisture level (~ 2%). Further analysis is needed to determine why some classes were more accurately classified than others.

When classifying areas with uniform moisture level, use of the GPS-derived surface *reflectivity* and *dispersion* features can significantly improve overall site classification accuracy as compared to using digital image data alone. When classifying areas with *different* SM levels, apart from the ground-penetrating nature of the ~19 cm wavelength GPS signal, no differentiation of regions based on soil moisture level can be achieved, given only shorter wavelength visible (or even mid- infrared) data. We note that increased classification accuracy is likely to be greater than reported here when combining these GPS features with traditional grayscale orthoquad imagery, where surface water bodies are often indistinguishable from regions of forest or pasture.

Although we have used visible wavelength imagery in this study, our method is generally extensible to data sets with thermal bands (e.g. Landsat) or to panchromatic imagery. In general, the choice of classes may be tailored to the particular application, be it precision agriculture or hydrological studies, among others.

ACKNOWLEDGEMENTS

The authors wish to express our kind thanks to Dr. David Bosch of the U. S. Department of Agriculture, Southeast Watershed Research Laboratory, Tifton, Georgia for providing ground truth soil moisture data for the sites used in this study.

REFERENCES

[1] S. J. Katzberg and J. L. Garrison, "Utilizing GPS to Determine Ionospheric Delay Over the Ocean," *NASA Tech. Memo.*, TM-4750, 1996.

[2] J. L. Garrison, S. J. Katzberg, and C. T. Howell III, "Detection of Ocean Reflected GPS Signals: Theory and Experiment," *Proceedings of the IEEE Southeastcon '97*, Blacksburg, VA, pp. 290-294, 1997.

[3] D. Masters, S. J. Katzberg, and P. Axelrad, "Airborne GPS Bistatic Radar Soil Moisture Measurements During SMEX02," *Proceedings of the IEEE Intl. Geoscience and Remote Sensing Symposium (IGARSS)*, Toulouse, France, 21-25 July, 2003.

[4] P. Beckman and A. Spizzichino, *The Scattering of Electromagnetic Waves from Rough Surfaces*, Artech House, Inc., 1987.

[5] F. T. Ulaby, R. K. Moore, and A. K. Fung, *Microwave Remote Sensing, Active and* Passive, Vol. 1, Artech House, 1981.

[6] T. Schmugge, T. J. Jackson, W. P. Kustas, and J. R. Wang, "Passive Microwave Remote Sensing of Soil Moisture: Results from HAPEX, FIFE and MONSOON 90," *ISPRS Journal of Photogrammetry and Remote Sensing*, 47, pp. 127-143, 1992.

[7] E. G. Enjoku, W. J. Wilson, S. H. Yueh, S. J. Dinardo, F. K. Li, T. J. Jackson, V. Lakshmi, and J. Bolton, "Observations of Soil Moisture Using a Passive and Active Low-Frequency Microwave Airborne Sensor During SGP99," *IEEE Transactions on Geoscience and Remote Sensing*, Vol. 40, No. 12, pp. 2659 – 2673, 2002.

[8] M. S. Grant and S. J. Katzberg, "Combined GPS Reflected Signal and Visual Imagery for Unsupervised Clustering and Terrain Classification," *Proceedings of the IEEE SoutheastCon 2004*, Greensboro, NC, pp. 370-377, March 26-29, 2004.

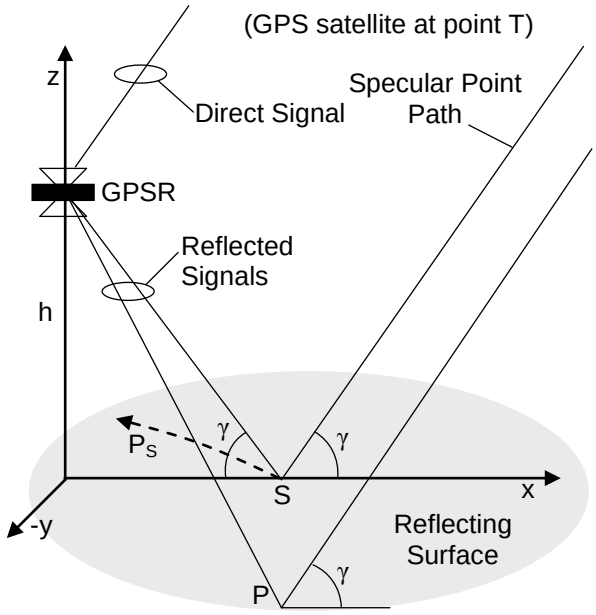

Fig. 1. Basic GPS remote sensing geometry showing simultaneous measurement of direct and surface-reflected satellite signals.

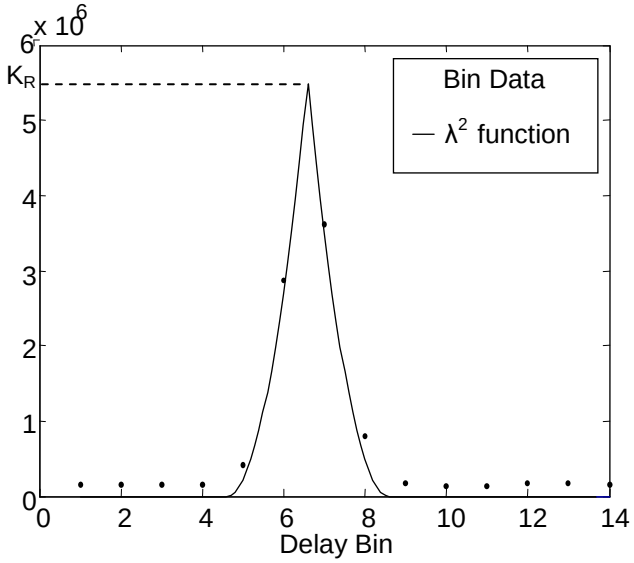

Fig. 2. Set of delay bin correlator measurements for a typical surface-reflected signal with estimated correlation peak, K_R, near delay bin 6.

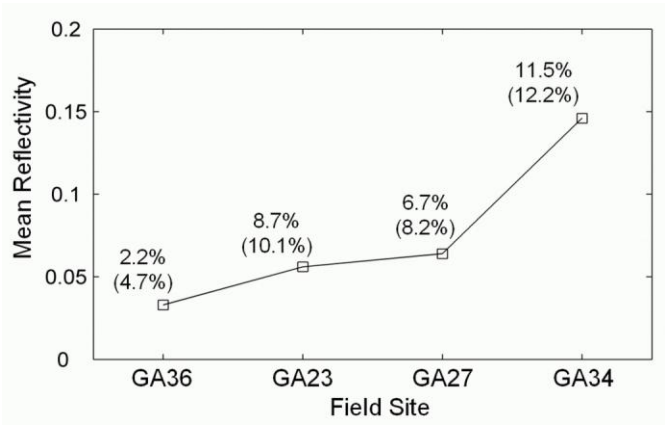

Fig. 3. Mean reflectivity of each field site. Percent soil moisture is given for 3 cm and 5 cm (in parentheses) soil depths.

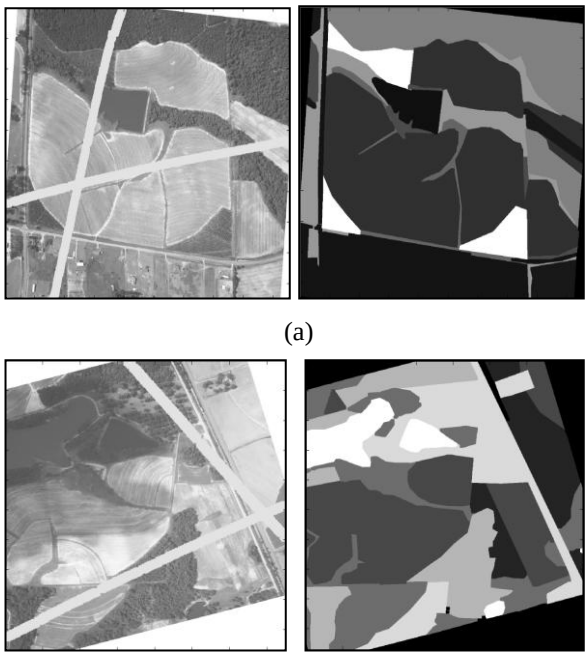

(a)

(b)

Fig. 4. Rectified images (left) showing specular point ground truth tracks for sites GA23 (a) and GA34 (b) and associated segmentation maps (right).

TABLE I. % CLASSIFICATION ACCURACY

Site No.	V	VR	VRD	Improvement with GPS
34	87.4	90.1	88.1	0.7
27	55.0	59.1	60.6	5.6
36	64.9	76.8	82.2	17.3
23	49.7	61.5	70.5	20.8

Classification cases are visible bands (V), visible plus GPS reflectivity (VR), and visible plus GPS reflectivity and dispersion (VRD). 'Improvement with GPS' is the difference between case 'VRD' and case 'V.'

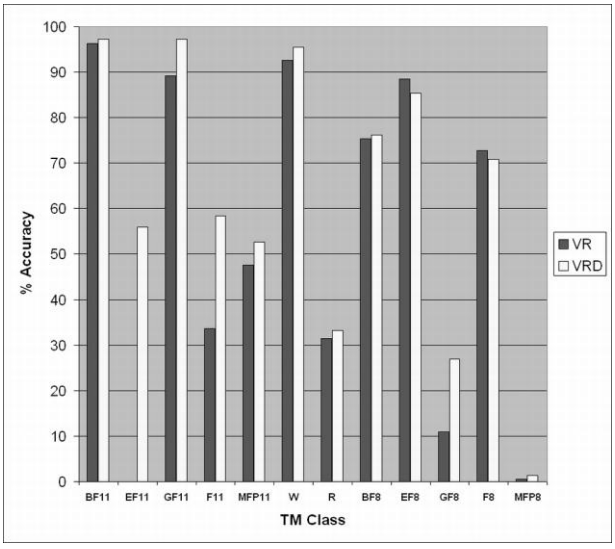

Fig. 5 Classification of sites GA23 (SM ~ 8%) and GA34 (SM ~ 11%) with common visible classes: 'Bare Field' (BF), 'Emergent Field' (EF), 'Grass Field' (GF), 'Forest' (F) and 'Mixed Forest/Pasture' (MPF), 'Water' (W), and 'Roads' (R). Classification cases are visible bands plus reflectivity (VR) and visible plus reflectivity and dispersion (VRD).